RESEARCH NEWS

Molecular Beam Epitaxial Growth of Topological Insulators

Xi Chen,* Xu-Cun Ma, Ke He, Jin-Feng Jia, and Qi-Kun Xue*

With the molecular beam epitaxy technique, layer-by-layer growth of atomically flat topological insulator Bi$_2$Te$_3$ and Bi$_2$Se$_3$ thin films has been realized on Si(111) and graphene substrates, respectively. The growth criteria by which intrinsic topological insulators can readily be obtained is established. By using *in situ* angle-resolved photoemission spectroscopy and scanning tunneling microscopy measurements, the band structure and surface morphology of Bi$_2$Te$_3$ and Bi$_2$Se$_3$ thin films of different thickness can be studied. Molecular beam epitaxy technique was shown to not only provide an excellent method to prepare high quality topological insulators but show possibilities of engineering their electronic and spin structures as well, which is of significant importance for potential applications of topological insulators based on well-developed Si technology.

1. Introduction

The recent theoretical prediction and experimental realization[1–14] of topological insulators have generated intense interest in this new state of quantum matter from both materials science and condensed matter physics. The strong spin-orbit coupling in these materials gives rise to the novel topological insulators in two and three dimensions in the absence of an external magnetic field. The surface states of three-dimensional (3D) topological insulators such as Bi$_2$Se$_3$,[12] Bi$_2$Te$_3$,[13] and Sb$_2$Te$_3$[14] consist of a single Dirac cone.[9] Crossing of the two surface state branches with opposite spins in the materials is fully protected by the time-reversal symmetry at the Dirac points, which cannot be destroyed by any time-reversal invariant perturbation. Such spin-helical states are expected to bring forward exotic physics, such as magnetic monopole[15] and Majorana fermions.[16,17]

The topological insulators are characterized by a bulk energy gap and the metallic surface states protected by time-reversal symmetry. For an intrinsic topological insulator, the Fermi level of the material resides in the bulk energy gap and thus only intersects the topological surface states. However, so far the topological insulator single-crystal samples prepared by the self-flux method, such as bulk Bi$_2$Te$_3$ and Bi$_2$Se$_3$, are all strongly doped

by the presence of vacancies and anti-sites defects. Angle-resolved photoemission spectroscopy (ARPES)[11–13,18–20] revealed large bulk electron pockets near Fermi level in these samples. It means that the novel physical properties of topological insulators, which are contributed from the topological surface states, are covered by the unwanted bulk carriers.

Further improvement in material quality by reducing the Se (Te) vacancies is highly challenging: it requires significant bulk diffusion of Se (Te) atoms in the quartz tube where the crystal forms. This process is difficult because of the very volatile nature of Se or Te molecules compared to Bi. To reduce the bulk electron carriers and move the Fermi level into the bulk gap, a great number of carriers of opposite sign were introduced by extremely heavy doping with Sn atoms in Bi$_2$Te$_3$[13] and Ca atoms in Bi$_2$Se$_3$.[18,20] However lowering of the crystalline quality and carrier mobility is unavoidable in this process. A more promising approach to achieve a true bulk insulator with high quality is to grow the topological insulator films by molecular beam epitaxy (MBE). The MBE-grown films not only reveal the intrinsic topological surface states in the cleanest manner, but also pave the road for future device applications involving topological insulators. The topological and thermoelectric properties of MBE-grown films make them strong candidates as the core components in multifunctional heterostructures for quantum computation, spintronics, and local chip cooling. In this Research News, we will give an overview on the recent developments of MBE preparation of topological insulator films.

2. MBE Growth of Bi$_2$Te$_3$

Bi$_2$Te$_3$ crystal has a rhombohedral structure, as schematically shown in **Figure 1**a. Along the [111] crystallographic direction, the five atomic layers with a stacking sequence of Te(1)-Bi-Te(2)-Bi-Te(1) form a quintuple layer (QL). The thickness of a QL is 10.17 Å and the lattice constant in the *a–b* (111) plane is 4.38 Å. A QL is terminated by a Te(1) atomic layer on both sides. The interaction between two adjacent QLs is basically van der Waals type, which is much weaker than the covalent bonding between two atomic layers within a QL. Therefore, a Bi$_2$Te$_3$ crystal always shows a Te-terminated surface due to its rather low surface energy.

The Bi$_2$Te$_3$ film has been successfully grown on Si(111)–(7 × 7) substrate.[21] The critical growth parameters are the Te$_2$/Bi flux ratios (θ) and the substrate temperature (T$_{Si}$). The optimal conditions for layer-by-layer growth of bulk insulating Bi$_2$Te$_3$ films

Prof. X. Chen, Prof. J.-F. Jia, Prof. Q.-K. Xue
Department of Physics
Tsinghua University
Beijing 100084, China
E-mail: xc@mail.tsinghua.edu.cn; qkxue@mail.tsinghua.edu.cn
Prof. Xu-Cun Ma, Dr. K. He, Prof. Q.-K. Xue
Institute of Physics
Chinese Academy of Sciences
Beijing 100190, China

Materials
Views

www.MaterialsViews.com

ADVANCED
MATERIALS

www.advmat.de

RESEARCH NEWS
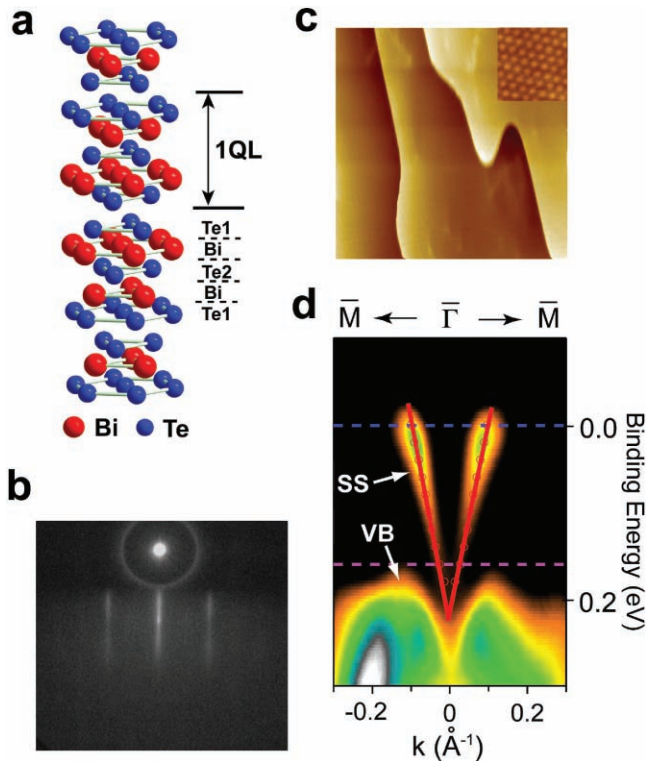
Figure 1. MBE growth of Bi_2Te_3. a) The schematic crystal structure of Bi_2Te_3. b) The RHEED patterns of a Bi_2Te_3 film. c) STM image of the 80-nm-thick film. All the steps seen in the image are 10.17 Å in height, corresponding to 1 QL. The image scale is 0.5 μm × 0.5 μm. The insert is an atomically resolved STM image (2.5 nm × 2.5 nm). d) ARPES intensity map of a Bi_2Te_3 film. The thickness is 80 QL. Reproduced with permission.[21]

were established by a systematic investigation of the growth dynamics, surface morphology and thickness-dependent electronic structure with reflection high-energy electron diffraction (RHEED), scanning tunneling microscopy (STM) and ARPES. The intrinsic topological insulator could be readily achieved under highly Te-rich condition ($\theta = 8 - 20$) with the substrate temperature satisfying $T_{Bi} > T_{Si} \geq T_{Te}$. Here, T_{Bi} and T_{Te} are the temperatures of Bi and Te Knudsen cells, which were used to precisely control the deposition flux (thus the flux ratio) of Bi and Te. The former not only assures the nucleation of the Bi_2Te_3 phase, according to the phase diagram, but also minimizes the formation of Te vacancy, which is difficult in self-flux method. Under Te-rich condition, there always exist extra Te molecules on the growing front. However, these molecules cannot be incorporated into the film and will desorb since $T_{substrate} > T_{Te}$. Figure 1b shows the time evolution of the intensity of RHEED (0,0) steak of the Bi_2Te_3 film under the optimal growth conditions. The clear RHEED intensity oscillation recorded during film deposition indicates an ideal layer-by-layer growth, where each period of the oscillations corresponds to the deposition of one QL of Bi_2Te_3.

The RHEED oscillation at different growth conditions indicates that the growth rate is only dependent on the Bi flux. This implies that under the condition of $T_{Si} \geq T_{Te}$, the Te_2 molecular beam does not stick to the 1 × 1-Te surface and the film does

not grow without simultaneous supply of the Bi atomic beam. This is important since it sets the lowest substrate temperature for possible stoichiometric growth of Bi_2Te_3. Below this limit, the Te atoms may no longer desorb from the 1 × 1-Te surface, leading to a situation similar to that in the methods such as co-deposition or bulk crystal growth.

A typical large-scale STM image of a 80-nm-thick film grown under the same condition is shown in Figure 1c. The atomically flat morphology is immediately evident. To illustrate the quality of the films, we carried out ARPES measurements. Figure 1d shows the band structure taken along the Γ–M direction of a 80-nm-thick Bi_2Te_3 film grown with a Te_2/Bi flux ratio of 13 at a substrate temperature of 543 K. A linearly dispersed band is clearly seen near Fermi level in Figure 1d. It is the mass-less Dirac-like surface states (SS), in agreement with previous theoretical predictions[9] and recent ARPES measurements on the cleaved (111) surface of the bulk crystal.[13] The broad "M"-shape features at the bottom are valence band (VB). It is to note that the bulk conduction bands (CBs) which can be observed in the undoped Bi_2Te_3 bulk crystals made by self-flux method[13] are completely absent at the Fermi level, indicating that the as-grown films made by MBE are indeed an intrinsic topological insulator.

The topological properties of Bi_2Te_3 have been studied by STM.[22] The STM images show the standing waves of the nontrivial surface states of topological insulator Bi_2Te_3 formed by the scattering of the topological states off Ag impurities and step edges on the Bi_2Te_3 surface. By studying the voltage dependent standing wave patterns, energy dispersion can be determined, which confirms the Dirac cone structure of the topological states. It has been shown that, very different from the conventional surface states, backscattering of the topological states by nonmagnetic impurities is completely suppressed. The absence of backscattering is a spectacular manifestation of the time-reversal symmetry, which offers a direct proof of the topological nature of the surface states.

3. MBE Growth of Bi_2Se_3

Bi_2Se_3 can also be grown on Si(111)-7 × 7 substrate. However a Bi-√3 × √3 reconstructed layer has to be grown first to avoid the formation of disordered silicon selenides at the interface. Nevertheless, the resulted Bi_2Se_3 films are not satisfying. Especially in the very thin regime (several QLs), the films show rather broad ARPES spectra and are strongly electron-doped.

On double-layer graphene formed on the commercial 6H-SiC(0001) substrates,[23] high quality Bi_2Se_3 thin films have been prepared. Graphene has a layered structure and is chemically inert due to the strong bonding of carbon atoms, which can not only greatly suppress the interface reaction between the reactive selenium atoms and the SiC substrate but also avoid the strain induced by the large lattice mismatch between Bi_2Se_3 and the substrate. As a result, the Bi_2Se_3 films exhibit atomically sharp interface with the substrate and less dislocations in growth. Similar to Bi_2Te_3, the layer-by-layer growth conditions of Bi_2Se_3 can be established by RHEED, STM and ARPES. The optimal growth can be achieved under Se-rich atmosphere (Se/Bi beam flux ratio $\theta \geq 10$) and $T_{Bi} > T_{substrate} > T_{Se}$ (T_{Bi}, $T_{substrate}$

RESEARCH NEWS
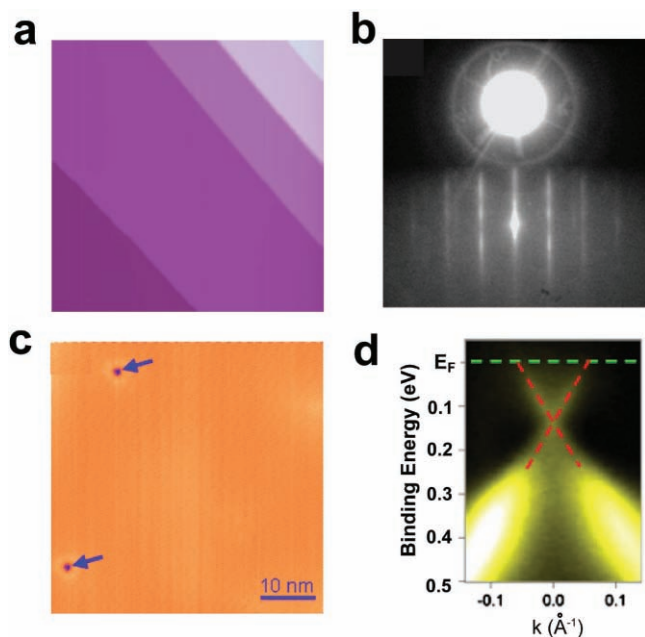
Figure 2. MBE growth of Bi$_2$Se$_3$. a) STM image of a 26 QL Bi$_2$Se$_3$ film acquired at a sample bias 1.0 V. b) RHEED pattern along Γ-K direction. c) STM image (10 mV) showing the Se vacancies (the blue arrows). d) ARPES intensity map of the 26 QL Bi$_2$Se$_3$ film along the Γ-K direction. The green dotted line indicates the Fermi level, and the red ones indicate the topological surface states. Reproduced from Ref. [23] Copyright 2010, AIP.

and T$_{Se}$ are the Bi-cell, Se-cell and substrate temperatures, respectively). The film shown in **Figure 2**a was grown at $\theta = 11$, T$_{Bi} = 550$ °C, T$_{Se} = 136$ °C, T$_{substrate} = 220$ °C and has a nominal thickness of 26 QL. The characteristic RHEED intensity oscillation recorded during film deposition indicates an ideal layer-by-layer growth (Figure 2b). Only two defects can be found in an area of 50 nm × 50 nm. The dominant defects are Se vacancies (the dark depressions in Figure 2c), which can be identified by their registry with respect to the topmost Se lattice. The areal defect density in this sample is $\sim 1.0 \pm 0.2 \times 10^{11}$ cm^{-2}, which is much lower than that on the cleaved samples. Further investigation indicates fewer vacancy defects if higher Se/Bi flux ratio is used. The electronic structure of the film is studied by ARPES and shown in Figure 2d. The Dirac cone (the dashed red lines) can be clearly seen, and the Dirac point is located at 130 meV below the Fermi level. The electronic pocket from the bulk conduction band observed in the cleaved crystals does not appear, suggesting that the film at this thickness is already a bulk insulator.

The Bi$_2$Se$_3$ films on graphene show much quicker development of the bulk insulating state than those on the √3 × √3-Bi/Si(111) substrate, suggesting more defects and poorer film quality in the latter case.

Landau quantization has been observed on the MBE Bi$_2$Se$_3$ thin films grown on graphene by using a low-temperature STM.[24] In particular, the zeroth Landau level, which is predicted to give rise to the half-quantized Hall effect for the topological surface states, was discovered. The existence of the

discrete Landau levels and the suppression of Landau levels by surface impurities strongly support the 2D nature of the topological states. These observations may eventually lead to the realization of quantum Hall effect in topological insulators.

4. Conclusions

The Te (Se)-rich growth dynamics and criterion for preparing high quality topological films of Bi$_2$Te$_3$ and Bi$_2$Se$_3$ by standard MBE technique have been established. The information can be applied to MBE growth of other topological materials such as Sb$_2$Te$_3$ and on other substrates. It is anticipated that the unconventional topological and electromagnetic properties of MBE-grown topological insulators can make them versatile components in spintronics.

[1] X.-L. Qi, S.-C. Zhang, *Phys. Today* **2010**, *63*, No.1, 33.
[2] J. E. Moore, *Nature* **2010**, *464*, 194.
[3] M. Z. Hasan, C. L. Kane, *Rev. Mod. Phys.* **2010**, *82*, 3045.
[4] L. Fu, C. L. Kane, E. J. Mele, *Phys. Rev. Lett.* **2007**, *98*, 106803.
[5] L. Fu, C. L. Kane, *Phys. Rev. B* **2007**, *76*, 045302.
[6] J. E. Moore, L. Balents, *Phys. Rev. B* **2007**, *75*, 121306.
[7] X.-L. Qi, T. L. Hughes, S.-C. Zhang, *Phys. Rev. B* **2008**, *78*, 195424.
[8] R. Roy, *Phys. Rev. B* **2009**, *79*, 195321.
[9] H. J. Zhang, C.-X. Liu, X.-L. Qi, X. Dai, Z. Fang, S.-C. Zhang, *Nat. Phys.* **2009**, *5*, 438.
[10] M. König, S. Wiedmann, C. Brüne, A. Roth, H. Buhmann, L. W. Molenkamp, X.-L. Qi, S.-C. Zhang, *Science* **2007**, *318*, 766.
[11] D. Hsieh, D. Qian, L. Wray, Y. Xia, Y. S. Hor, R. J. Cava, M. Z. Hasan, *Nature* **2008**, *452*, 970.
[12] Y. Xia, D. Qian, D. Hsieh, L. Wray, A. Pal, H. Lin, A. Bansil, D. Grauer, Y. S. Hor, R. J. Cava, M. Z. Hasan, *Nat. Phys.* **2009**, *5*, 398.
[13] Y. L. Chen, J. G. Analytis, J.-H. Chu, Z. K. Liu, S.-K. Mo, X.-L. Qi, H. J. Zhang, D. H. Lu, X. Dai, Z. Fang, S. C. Zhang, I. R. Fisher, Z. Hussain, Z.-X. Shen, *Science* **2009**, *325*, 178.
[14] D. Hsieh, Y. Xia, D. Qian, L. Wray, F. Meier, J. H. Dil, J. Osterwalder, L. Patthey, A. V. Fedorov, H. Lin, A. Bansil, D. Grauer, Y. S. Hor, R. J. Cava, M. Z. Hasan, *Phys. Rev. Lett.* **2009**, *103*, 146401.
[15] X.-L. Qi, R. Li, J. Zang, S.-C. Zhang, *Science* **2009**, *323*, 1184.
[16] L. Fu, C. L. Kane, *Phys. Rev. Lett.* **2008**, *100*, 096407.
[17] X.-L. Qi, T. L. Hughes, S. Raghu, S.-C. Zhang, *Phys. Rev. Lett.* **2009**, *102*, 187001.
[18] D. Hsieh, Y. Xia, D. Qian, L. Wray, J. H. Dil, F. Meier, J. Osterwalder, L. Patthey, J. G. Checkelsky, N. P. Ong, A. V. Fedorov, H. Lin, A. Bansil, D. Grauer, Y. S. Hor, R. J. Cava, M. Z. Hasan, *Nature* **2009**, *460*, 1101.

[19] D. Hsieh, Y. Xia, L. Wray, D. Qian, A. Pal, J. H. Dil, J. Osterwalder, F. Meier, G. Bihlmayer, C. L. Kane, Y. S. Hor, R. J. Cava, M. Z. Hasan, *Science* **2009**, *323*, 919.

[20] Y. S. Hor, A. Richardella, P. Roushan, Y. Xia, J. G. Checkelsky, A. Yazdani, M. Z. Hasan, N. P. Ong, R. J. Cava, *Phys. Rev. B* **2009**, *79*, 195208.

[21] Y.-Y. Li, G. Wang, X.-G. Zhu, M.-H. Liu, C. Ye, X. Chen, Y.-Y. Wang, K. He, L.-L. Wang, X.-C. Ma, H.-J. Zhang, X. Dai, Z. Fang, X.-C. Xie, Y. Liu, X.-L. Qi, J.-F. Jia, S.-C. Zhang, Q.-K. Xue, *Adv. Mater.* **2010**, *22*, 4002.

[22] T. Zhang, P. Cheng, X. Chen, J.-F. Jia, X.-C. Ma, K. He, L.-L. Wang, H.-J. Zhang, X. Dai, Z. Fang, X.-C. Xie, Q.-K. Xue, *Phys. Rev. Lett.* **2009**, *103*, 266803.

[23] C.-L. Song, Y.-L. Wang, Y.-P. Jiang, Y. Zhang, C.-Z. Chang, L.-L. Wang, K. He, X. Chen, J.-F. Jia, Y. Y. Wang, Z. Fang, X. Dai, X.-C. Xie, X.-L. Qi, S.-C. Zhang, Q.-K. Xue, X.-C. Ma, *Appl. Phys. Lett.* **2010**, *97*, 143118.

[24] P. Cheng, C.-L. Song, T. Zhang, Y.-Y. Zhang, Y.-L. Wang, J.-F. Jia, J. Wang, Y.-Y. Wang, B.-F. Zhu, X. Chen, X.-C. Ma, K. He, L.-L. Wang, X. Dai, Z. Fang, X.-C. Xie, X.-L. Qi, C.-X. Liu, S.-C. Zhang, Q.-K. Xue, *Phys. Rev. Lett.* **2010**, *105*, 076801.